THE ASTROPHYSICAL JOURNAL, 583:559–565, 2003 February 1

SUNYAEV-ZELDOVICH EFFECT IMAGING OF MACS GALAXY CLUSTERS AT $z > 0.5$

SAMUEL J. LAROQUE,[1] MARSHALL JOY,[2] JOHN E. CARLSTROM,[1,3] HARALD EBELING,[4]
MASSIMILIANO BONAMENTE,[5] KYLE S. DAWSON,[6] ALASTAIR EDGE,[7]
WILLIAM L. HOLZAPFEL,[6] AMBER D. MILLER,[8] DAISUKE NAGAI,[1]
SANDEEP K. PATEL,[9] AND ERIK D. REESE[6]
Received 2002 June 22; accepted 2002 October 10

ABSTRACT

We present 30 GHz interferometric Sunyaev-Zeldovich effect (SZE) measurements of a redshift-limited, X-ray–selected cluster sample from the Massive Cluster Survey (MACS). All eight of the high-redshift ($z > 0.5$, $\delta > -15°$) galaxy clusters were detected. Additional observations were made at 4.8 GHz with the Very Large Array to help constrain the amount of point source contamination to the SZE decrements. From SZE data alone, we derive electron temperatures in the range 5.5–18.5 keV and total masses between 1.5 and $2.6 \times 10^{14}\ h^{-1}\ M_\odot$ within a 65″ radius (0.28 h^{-1} Mpc at $z = 0.5$) for the eight clusters. Six of the clusters are MACS discoveries, while two (Cl 0016+1609 and MS 0451.6−0305) were detected by previous X-ray observations and have been recently observed with the *Chandra* observatory. The X-ray–derived temperatures and masses for Cl 0016+1609 and MS 0451.6−0305 are in good agreement with the SZE derived values. Strong detections of the SZE signal in this sample of MACS objects confirm that they are hot, massive clusters.

Subject headings: cosmic microwave background — cosmology: observations — galaxies: clusters: general — submillimeter — techniques: interferometric — X-rays: galaxies: clusters

On-line material: color figure

1. INTRODUCTION

Massive clusters of galaxies are believed to have formed through gravitational collapse of overdense regions in the primordial universe. The evolution of these overdensities to the massive systems seen today depends strongly on cosmological parameters, most notably the matter density of the universe, Ω_M, and the rms amplitude of fluctuations in the matter on a scale of 8 h^{-1} Mpc, σ_8. The existence of massive clusters at intermediate and high redshifts implies that formation of large structures began early and implies a low value of Ω_M (Bahcall & Fan 1998). The Massive Cluster Survey (MACS; Ebeling, Edge, & Henry 2001; H. Ebeling et al. 2003, in preparation) is designed to find such massive clusters. MACS combines the largest solid angle of any *ROSAT* All-Sky Survey cluster survey with a relatively low X-ray flux limit to maximize the number of cluster detections at redshifts $z > 0.3$. As of 2002 June, the MACS sample comprised 119 spectroscopically confirmed clusters, three-quarters of which were new discoveries.

We present detections of the Sunyaev-Zeldovich effect (SZE) toward all eight MACS clusters with redshift $z > 0.5$ and declination $\delta > -15°$ detected as of 2001 August (Table 1). These results represent a complete SZE follow-up of a redshift-limited, X-ray–selected sample of objects. Following the methods of Grego et al. (2001) and Joy et al. (2001), the SZE data are used to confirm the X-ray detections of all eight clusters and provide estimates of their gas temperature and mass. Six of the clusters in Table 1 are new MACS discoveries (H. Ebeling et al. 2003, in preparation); the remaining two had been extensively studied prior to their MACS detections (Henry et al. 1992; Donahue 1996; Neumann & Böhringer 1997; Reese et al. 2000) and are commonly known as Cl 0016+1609 and MS 0451.6−0305. For the remainder of this paper, the cluster names are abbreviated using only the first four digits of their right ascension.

Very Large Array (VLA) data for five of the MACS clusters are analyzed to constrain the positions and fluxes of faint point sources in the fields and determine what effect these sources have on the SZE mass and temperature measurements. In addition, we analyze data from the *Chandra X-Ray Observatory* to determine the electron temperature and total mass of Cl 0016 and use recent *Chandra* X-ray measurements of the temperature and mass of MS 0451 (M. Donahue et al. 2003, in preparation) to compare with the SZE results. The SZE observations and all data analysis are described in § 2, and § 3 contains the conclusions drawn from these data. Throughout this paper, the Hubble constant is parametrized in terms of h, where $H_0 \equiv 100\ h$ km s^{-1} Mpc^{-1}, and a ΛCDM universe with $\Omega_M = 0.3$ and $\Omega_\Lambda = 0.7$ is assumed. Uncertainties are reported at the 68% confidence level unless otherwise noted.

2. OBSERVATIONS AND DATA REDUCTION

2.1. *OVRO and BIMA Observations*

The SZE is the change in the observed brightness temperature of the cosmic microwave background (CMB)

[1] Department of Astronomy and Astrophysics, University of Chicago, Chicago, IL 60637.
[2] Department of Space Science, SD50, NASA Marshall Space Flight Center, Huntsville, AL 35812.
[3] Center for Cosmological Physics, Department of Physics, Enrico Fermi Institute, University of Chicago, Chicago, IL 60637.
[4] Institute for Astronomy, 2680 Woodlawn Drive, Honolulu, HI 96822.
[5] Physics Department, University of Alabama, Huntsville, AL 35899.
[6] Physics Department, University of California, Berkeley, CA 94720.
[7] Department of Physics, University of Durham, Durham DH1 3LE, UK.
[8] Physics Department, Columbia University, New York, NY 10027.
[9] National Academy of Sciences-NRC/NSSTC, SD-50, Huntsville, AL 35805.

TABLE 1
Cluster Observation Log

Cluster Name	Alternate Designation	Redshift[a]	Pointing Center (J2000.0) α	δ	On-Source Integration Time (hr) BIMA	OVRO
MACS J0018.5+1626	Cl 0016+1609[b]	0.544	00 18 34.6	16 26 18	43.0	100
MACS J0454.1−0300	MS 0451.6−0305[c]	0.550	04 54 10.8	−03 00 57	...	30.0
MACS J0647.7+7015	...	0.584	06 47 50.0	70 14 55	...	22.7
MACS J0717.5+3745	...	0.548	07 17 33.8	37 45 20	26.3	...
MACS J0744.8+3927	...	0.686	07 44 52.5	39 27 30	4.5	16.8
MACS J1149.5+2223	...	0.544	11 49 34.3	22 23 42	39.3	1.2
MACS J1423.8+2404	...	0.545	14 23 48.3	24 04 47	35.1	...
MACS J2129.4−0741	...	0.570	21 29 26.0	−07 41 28	...	23.6

Note.—Right ascension is given in hours, minutes, and seconds. Declination is given in degrees, arcminutes, and arcseconds.
[a] H. Ebeling et al. 2003, in preparation.
[b] Cf. Koo 1981.
[c] Cf. Henry et al. 1992.

radiation resulting from passage of CMB photons through the thermally ionized gas permeating a galaxy cluster (Sunyaev & Zeldovich 1972, 1980). Observations of the SZE were performed using centimeter-wavelength receivers equipped with cryogenically cooled high electron mobility transistor amplifiers (Carlstrom, Joy, & Grego 1996). These amplifiers are sensitive to radiation between 26 and 36 GHz, with typical receiver temperatures $T_{\rm rx} \sim 11$–20 K. The cluster pointing centers and on-source integration times are shown in Table 1; pointing centers are coincident with the cluster X-ray centers.

Observations of the six newly discovered MACS clusters were conducted using our centimeter-wave interferometric imaging system with the Berkeley Illinois Maryland Association (BIMA) and Owens Valley Radio Observatory (OVRO) millimeter-wave arrays in the summers of 2000 and 2001. Cl 0016 and MS 0451 were observed in the summers of 1994–1997 as a part of previous studies. (See Reese et al. 2000 for details of these observations.) At BIMA, nine 6.1 m dishes were used, each with a 6$'$.6 FWHM Gaussian response pattern. Most were placed in a compact configuration to maximize SZE sensitivity, with the remainder placed at longer baselines allowing point sources to be distinguished in the field. We used an 800 MHz band centered at 28.5 GHz, with typical system temperatures between 45 and 55 K (scaled to above the atmosphere). The data were reduced with the MIRIAD software package (Sault, Teuben, & Wright 1995). At OVRO, we used six 10.4 m telescopes with a 4$'$.2 FWHM Gaussian response pattern, using two 1 GHz bands centered at 28.5 and 30 GHz. Again, most telescopes were placed in a compact configuration while the remainder comprised longer baselines, and typical system temperatures were 45–55 K, scaled to above the atmosphere. The data were reduced using the MMA software package (Scoville et al. 1993). Further details regarding the instrument configurations are given in Reese et al. (2000).

In all cases, measurements were interleaved with observations of a bright point source at $\sim$25 minute intervals to facilitate monitoring of the response of the interferometer. Mars was used for amplitude calibration, with its adopted brightness temperature taken from the Rudy (1987) Mars model. Data were flagged from baselines at which one telescope was shadowed by another, when a cluster observation was not bracketed by observations of the bright point source, when observations of the bright point source indicated poor atmospheric coherence, and when there was spurious correlation.

Point sources in the fields were identified by creating images with DIFMAP (Pearson et al. 1994) using only long baselines (≥ 2 kλ) and natural weighting ($\propto \sigma^{-2}$). The approximate positions and fluxes of these point sources are used as inputs to the model fitting described in the next section.

2.2. *SZE Data Analysis*

The OVRO and BIMA data are analyzed directly in the Fourier (*u*-*v*) plane, where the noise characteristics and spatial filtering of the interferometer are well understood. Point sources are modeled as delta functions, and the cluster is modeled as an isothermal spherical β model (Cavaliere & Fusco-Femiano 1976, 1981) given by

$$n_e(r) = n_{e0}\left(1 + \frac{r^2}{r_c^2}\right)^{-3\beta/2}, \qquad (1)$$

where n_{e0} is the central electron density, r_c is the core radius of the intracluster medium, and β is a power-law index. The SZE temperature change (a decrement at 30 GHz) has the form $\Delta T \propto f(\nu) \int n_e T_e dl$, where n_e and T_e are the electron density and temperature of the cluster and $f(\nu)$ contains the SZE frequency dependence. Combining this with equation (1), the SZE signal has an angular dependence given by

$$\Delta T(\theta) = \Delta T_0\left(1 + \frac{\theta^2}{\theta_c^2}\right)^{(1-3\beta)/2}, \qquad (2)$$

where $\theta = r/D_A$, $\theta_c = r_c/D_A$, D_A is the angular diameter distance of the cluster, and ΔT_0 is the temperature decrement at the cluster center.

The model fitting and mass calculations closely follow Grego et al. (2001), where a model consisting of equation (2) multiplied by the response pattern of the telescope is constructed in image space, then fast Fourier transformed to *u*-*v* space, where it is compared with the data using the χ^2 statistic. The best-fit cluster centroid position, point source positions, and point source fluxes are found by minimizing χ^2 using a downhill simplex algorithm (Press et al. 1992). These parameters are fixed at their best-fit positions, and a three-dimensional grid is formed by stepping through a range of θ_c, β, and ΔT_0. At each grid point, the number of electrons in a given volume and, subsequently, the cluster gas mass can be calculated by determining n_{e0} from equations (1) and (2), then integrating over the β model. Assuming that the gas is in hydrostatic equilibrium (HSE) with the cluster potential, the total mass and gas mass fraction are then calculated at each grid point from the equation

$$M_{\rm tot}(r) = \frac{3kT_e}{G\mu m_p}\beta r \frac{(r/r_c)^2}{1+(r/r_c)^2}\ , \tag{3}$$

where m_p is the proton mass and $\mu(=0.61)$ is the mean molecular weight. The masses are calculated at a radius of 65″ (corresponding to a physical radius of 0.28 h^{-1} Mpc at $z = 0.5$), where the SZE data best constrain the cluster gas mass fraction (Grego et al. 2001). The mass calculations described here require knowledge of the cluster's electron temperature, however, and since T_e is not known a priori, a range of temperatures is stepped through and the above procedure is carried out for each T_e. Total mass values for which the χ^2 statistic is within the 68% confidence interval ($\Delta\chi^2 = 1$) in the (θ_c, β, ΔT_0) grid are retained for each T_e. Following Joy et al. (2001), the electron temperature of the cluster is then taken to be that which yields a best-fit gas mass fraction (f_g) equal to the mean value determined from a sample of 18 clusters presented in Grego et al. (2001). This mean is $\bar{f}_g(r_{500}) = 0.081^{+0.009}_{-0.011}$ for an $\Omega_M = 0.3$, $\Omega_\Lambda = 0.7$ universe, where r_{500} is the radius at which the cluster's total mass density is 500 times the critical mass density of the universe. The uncertainty in the mean gas mass fraction reported in Grego et al. (2001) is smaller than the uncertainty on a single measurement by a factor of $n^{1/2}$, where n is the number of objects in the sample. For this work, we determine the uncertainty in T_e using $\bar{f}_{\rm single}(r_{500}) = 0.081^{+0.038}_{-0.047}$. The gas mass fraction measurements within 65″ are scaled to r_{500} using scaling relations from gas dynamical simulations (Evrard, Metzler, & Navarro 1996; Evrard 1997) for comparison with the Grego et al. (2001) result. The electron temperatures consistent with the 1 σ uncertainties in $\bar{f}_{\rm single}(r_{500})$ and the corresponding total cluster masses within 65″ are reported in Table 2.

2.3. *VLA Observations*

Undetected point sources, if unaccounted for, can interfere with the SZE decrement and subsequently distort the SZE-derived masses and temperatures. The high point source sensitivity of the VLA is therefore used to determine the position of point sources in the fields with fluxes below BIMA and OVRO's detection threshold. The VLA observations were made in the 4.8 GHz band, where the 9′ FWHM field of view is well matched to BIMA's. MACS 0647, 0717, 0744, 1149, and 1423 were observed by the VLA on 2001 November 27 with the dishes in the D configuration. All clusters were observed for 1.5 hr, achieving an rms noise level of ~25–30 μJy for each map. As with the OVRO and BIMA observations, measurements of a bright point source were interleaved at ~25 minute intervals to monitor the interferometer's response.

The VLA data reduction is similar to that for the OVRO and BIMA data. Data were flagged due to shadowing, poor atmospheric coherence, and spurious correlation; data were also flagged if a source observation was not bracketed by observations of a bright point source. The data were reduced with the MIRIAD software package. The bright source 0137+331 was used for amplitude calibration. Its adopted flux is recorded in the VLA Calibrator Flux Density Database.[10] After reducing the data, MIRIAD was used to establish the position of each bright (>6 σ) point source in the VLA maps.

The number of sources in each VLA map ranges from just one (MACS 0744) to as many as six (MACS 0717 and 1423). If a greater than 3 σ signal appears at the VLA point source position in the OVRO or BIMA maps, the source is considered to be detected and its 30 GHz position and flux are fit accordingly. The 3 σ level is considered statistically significant given that the point source position is already established by the VLA data. Table 3 lists the rms noise levels at 30 GHz for maps with u-v radius greater than 2 kλ (for clusters with both OVRO and BIMA data, we choose the lesser rms), point source positions, and beam-corrected fluxes at 30 GHz and 4.8 GHz. (Note that there are no VLA data for MS 0451 or MACS 2129.) The 4.8 GHz data for Cl 0016 are from Moffet & Birkinshaw (1989).

In most cases, there is not a greater than 3 σ signal on the 30 GHz map at the VLA positions. To determine the effect of point sources undetected in the 30 GHz data, we allow the SZE decrement and the fluxes of the undetected point sources to vary while keeping r_c, β, the cluster position, and the VLA-determined positions of the undetected point sources fixed at their best-fit values. Inclusion of the additional point sources causes a change in the decrement of between 2% and 10% for the six clusters. This translates to

[10] See http://aips2.nrao.edu/vla/calflux.html.

TABLE 2

CLUSTER PROPERTIES DERIVED FROM SZE MEASUREMENTS

Cluster Name	Cluster Position[a] (arcsec) $\Delta\alpha$	$\Delta\delta$	$T_e^{\rm SZE}$ (keV)	$M_{\rm tot}^{\rm SZE}[<65'']$ ($10^{14}\ h^{-1}\ M_\odot$)	$T_e^{X\text{-ray}}$ (keV)	$M_{\rm tot}^{\rm X\text{-ray}}[<65'']$ ($10^{14}\ h^{-1}\ M_\odot$)
Cl 0016	−20.5	−14.1	$12.7^{+7.6}_{-2.3}$	$1.9^{+1.2}_{-0.4}$	$10.7^{+0.8}_{-0.7}$	1.8 ± 0.1
MS 0451	10.7	3.9	$13.5^{+8.1}_{-2.5}$	$2.1^{+1.2}_{-0.4}$	10.6 ± 0.8[b]	2.1 ± 0.2[b]
MACS 0647	2.9	1.2	$5.5^{+3.2}_{-1.0}$	$2.6^{+1.5}_{-0.5}$	...	...
MACS 0717	−44.3	−1.4	$18.5^{+11.2}_{-3.5}$	$2.1^{+1.3}_{-0.4}$	...	...
MACS 0744	−2.8	3.3	$17.9^{+10.8}_{-3.4}$	$2.3^{+1.4}_{-0.5}$	...	...
MACS 1149	5.9	14.6	$10.9^{+6.5}_{-2.0}$	$1.5^{+0.9}_{-0.3}$	...	...
MACS 1423	8.1	5.9	$13.6^{+8.2}_{-2.5}$	$1.6^{+1.0}_{-0.3}$	...	...
MACS 2129	15.6	3.2	$10.7^{+6.3}_{-2.0}$	$1.8^{+1.0}_{-0.3}$	...	...

[a] Offsets from radio pointing center (Table 1).

[b] M. Donahue et al. 2003, in preparation.

TABLE 3
Radio Point Sources

Cluster Name	rms Noise (mJy beam^{-1})	Cluster Position[a] (arcsec) $\Delta\alpha$	$\Delta\delta$	Flux (30 GHz)[b] (mJy)	Flux (4.8 GHz)[b] (mJy)
Cl 0016	0.240	−60	−333	9.07	84.5
MS 0451	0.062	165	−29	1.88	...
MACS 0647	0.107	...	...	...	...
MACS 0717	0.166	40.3	−57.3	2.70	3.17
	...	86.9	−122.4	1.60	5.81
MACS 0744	0.107	...	...	...	...
MACS 1149	0.154	−166.0	−13.2	3.01	4.01
MACS 1423	0.160	−7.8	−4.2	1.58	4.40
	...	−48.5	−64.3	0.58	2.72
MACS 2129	0.110	63.0	−62.4	0.83	...

[a] Offsets from radio pointing center (Table 1).
[b] Beam-corrected.

no more than a 5% uncertainty in the T_e and $M_{\rm tot}$ calculations described in the previous section, which is small in comparison with statistical uncertainties.

2.4. *Chandra Data Analysis*

Chandra X-ray data from the clusters Cl 0016 and MS 0451 are analyzed to obtain independent measurements of their temperature and mass. Comparison between the X-ray and SZE-derived properties provides a check for consistency in our SZE method.

Cl 0016 was observed with the *Chandra* Advanced CCD Imaging Spectrometer (ACIS) detector on 2000 August 18 with a total useful exposure time of 67,411 s. The light curve for background flares was examined using the CIAO script *analyze_ltcrv*; all of the data points were within 3 σ of the mean, so no data were excluded due to flares. For the spectral analysis, X-ray events were extracted from a circular region with radius 1$'$.5 centered on the cluster, which was located at the standard aim point on ACIS-I chip 3. The X-ray background was determined by extracting events (using the same circular regions) from adjacent chips in the ACIS-I array. The background rates measured on the adjacent chips were consistent within 5%. We averaged the different background measurements and include a 5% systematic uncertainty in the background rate in our analysis. The on-source count rate (cluster plus background) was 0.2410 ± 0.0019 counts s^{-1}, and the average background rate was $1.313 \pm 0.044 \times 10^{-2}$ counts s^{-1} (1 σ errors) in the 0.6–7.0 keV energy band.

To determine the temperature of the cluster, the ACIS-I3 data in the energy band 0.6–7.0 keV were fit to an optically thin thermal plasma model (Mewe, Gronenschild, & van den Oord 1985; Mewe, Lemen, & van den Oord 1986; Kaastra 1992) including the effects of Galactic absorption (Morrison & McCammon 1983) and using the abundances of Anders & Grevesse (1989). The standard calibration files in *Chandra* CALDB2.12 were used, including low-energy corrections to the ACIS quantum efficiency.[11] The fitting was performed using XSPEC, with data grouped to contain a minimum of 25 counts bin^{-1} in the pulse invariant (PI) detector channels. We found a good fit with $\chi^2 = 266$ for 252 degrees of freedom. The resulting temperature is $10.7^{+1.3}_{-1.2}$ keV, with a fractional metal abundance of 0.2 ± 0.1 solar and an H I column density of $5.8^{+1.5}_{-1.4} \times 10^{20}$ atoms cm^{-2} (statistical uncertainties at 90% confidence). These parameters are comparable to the values derived by Worrall & Birkinshaw (2003) from *XMM-Newton* measurements of Cl 0016: $kT = 9.13^{+0.49}_{-0.44}$ keV, abundance $= 0.22^{+0.07}_{-0.065}$ solar, and $N_{\rm H} = 4.3 \pm 0.6 \times 10^{20}$ atoms cm^{-2} (*XMM-Newton* statistical uncertainties at 95% confidence).

To determine the total mass of Cl 0016, we prepared a cluster image with exposure map corrections applied. The image was blocked by a factor of 4 to a pixel size of 1$''$.97 × 1$''$.97, and X-ray bright point sources in the field were excluded. This image was then used in the two dimensional surface brightness modeling. We again assume that the cluster is described by an isothermal β model and fit the X-ray surface brightness to the function

$$S_{\rm X}(\theta) = S_{\rm X0}\left(1 + \frac{\theta^2}{\theta_c^2}\right)^{(1-6\beta)/2} + B\ . \tag{4}$$

The first term arises from integrating the X-ray emissivity along the line of sight, where $S_{\rm X0}$ is the central X-ray surface brightness. The second term, B, is the X-ray background, assumed constant over the fitting region. From this fit, θ_c and β are determined; the best-fit values are $\theta_c = 37''.6$ and $\beta = 0.696$. Then, under the HSE assumption, the total gravitational mass of the cluster is derived using equation (3). Within r_{500}, which corresponds to a physical radius of 0.96 h^{-1} Mpc (3$'$.6) at $z = 0.544$, we find a total gravitational mass of $M_{\rm tot}(r_{500}) = 7.6^{+1.4}_{-1.3} \times 10^{14}\ h^{-1}\ M_\odot$ (statistical uncertainties at 90% confidence). The shape parameters θ_c and β are sufficiently well constrained by the X-ray data that the major contribution to the mass uncertainty is from uncertainty in the temperature. This is the only source of uncertainty accounted for in the mass result presented here.

MS 0451 was observed by *Chandra* on 2000 October 18. The observations and data reduction are described in M. Donahue et al. (2003, in preparation). They find a temperature of $10.6^{+1.4}_{-1.2}$ keV and a total gravitational mass of $8.3^{+1.7}_{-1.4} \times 10^{14}\ h^{-1}\ M_\odot$ within r_{500} for this cluster (statistical uncertainties again at 90% confidence).

[11] Go to http://cxc.harvard.edu/cal/Links/Acis/acis/Cal_prods/qeDeg for more information.

3. RESULTS AND CONCLUSIONS

Synthesized images of the SZE toward the eight MACS clusters are presented in Figure 1: image properties are detailed in Table 4. The SZE toward each cluster is detected with high significance, and the positions of the SZE and X-ray centroids are consistent (Tables 1 and 2). As shown in Table 2, the SZE-determined masses within a 65″ radius are between 1.5 and $2.6 \times 10^{14}\ h^{-1}\ M_{\odot}$, indicating that these are indeed massive clusters. The X-ray masses listed in Table 2 have been recalculated at a radius of 65″ using the derived values from § 2.4 in equation (3); this facilitates comparison with the SZE-derived masses. Note that the temperature and mass uncertainties for Cl 0016 and MS 0451 reported in Table 2 are at the 68% confidence level for consistency with the SZE results. The X-ray determined masses and temperatures of Cl 0016 and MS 0451 are in good agreement with their SZE-derived values. Although the uncertainties in the SZE measurements are much larger than the X-ray uncertainties, the agreement between the X-ray and SZE results for Cl 0016 and MS 0451 confirms that for an assumed f_g, reasonable estimates of cluster temperatures and masses can be obtained from SZE data alone. MACS 0717 and 0744 have the highest SZE-derived temperatures in this sample at $18.5^{+11.2}_{-3.5}$ and $17.9^{+10.8}_{-3.4}$ keV, respectively; if confirmed by X-ray measurements, these would be among the hottest clusters known (cf. Markevitch et al. 2002, who find a temperature of $14.8^{+1.7}_{-1.2}$ keV for the cluster 1E 0657−56). Such high temperatures in relaxed clusters would be unusual. *Chandra* follow-up observations in progress will reveal more about the structure and possible merger history of these two objects.

We investigate the effect of cluster asphericity and orientation on the SZE-derived temperature. Clearly, clusters have a range of ellipticities and inclination angles (Mohr et al. 1995) that strongly affect the projected X-ray and SZE morphology. We consider first the limiting case of a large prolate cluster that is oriented along the line of sight. Viewed in projection, the X-ray emission from such a cluster will appear to have a higher surface brightness than that of clusters observed at lower inclination angles. Although this effect could lead to a selection bias favoring the detection of clusters elongated along the line of sight, MACS is essentially immune to this bias owing to the fact that, at the low angular resolution of the *ROSAT* All-Sky Survey data used in the X-ray selection process, all clusters at $z > 0.5$ appear essentially pointlike, irrespective of their true or projected X-ray morphology. The effect variations in inclination angle would have on the SZE-derived temperature is evaluated by applying both spherical and ellipsoidal models to the SZE data and comparing the results. We assume a large cluster with angular core radius 50″ at redshift $z = 0.5$, $\beta = 2/3$, and for the ellipsoidal model, an intrinsic major axis/minor axis ratio of $2^{1/2}$, beyond which the dark matter distribution in the cluster becomes unphysical (Grego et al. 2000). The SZE temperature derived with the spherical model is found to be 10% higher than the temperature derived with the ellipsoidal model. Therefore, SZE temperatures derived with a spherical model will overestimate the temperature of prolate clusters that are oriented along the line of sight. For completeness, the other limiting case of a prolate cluster oriented perpendicular to the line of sight is also considered. Applying the same models, it is found that the temperature from the spherical model is 20% lower than the temperature derived from the ellipsoidal model. Accounting for cluster asphericity and orientation therefore leads to an additional 10%–20% uncertainty in the cluster temperatures. This may be viewed as a lower limit, however, as the more complex morphology and substructure in real clusters may have a greater systematic impact on the results presented here.

These SZE measurements of a complete redshift-selected, flux-limited X-ray sample of objects from MACS confirms that they are hot, massive clusters, a finding which continues to favor a low Ω_M universe in which structure develops early. *Chandra* observations of all of these clusters are in progress and will yield tighter constraints on their angular diameters, temperatures, and masses.

We thank Rick Forster, Dick Plambeck, Steve Scott, David Woody, and the staff of the BIMA and OVRO observatories for their outstanding support. We also thank Diana Worrall and Megan Donahue for providing the results of their observations prior to publication. We are grateful for the scheduling of time at the VLA in support of this project. S. L. and E. R. gratefully acknowledge support from NASA GSRP Fellowships NGT5-50173 and NGT8-52906, respectively. A. E. thanks the Royal Society for generous support. A. M. was supported by Hubble Grant ASTR/HST-HF-0113. This work is supported in part by NSF grant 0096913, NASA grants NAG5-7986 and NAG5-8253, and the David and Lucile Packard Foundation. Radio astronomy at the BIMA millimeter array is supported by NSF grant AST 96-13998. The OVRO millimeter array is supported by NSF grant AST96-13717.

TABLE 4

Properties of Cluster Images

Panel	Cluster	Observatory	Resolution (arcsec × arcsec)	Map rms (μJy beam^{-1})	Map rms (μK)
(1)	Cl 0016	BIMA	81 × 101	250	46
(2)	MS 0451	OVRO	48 × 70	70	31
(3)	MACS 0647	OVRO	53 × 57	60	30
(4)	MACS 0717	OVRO	95 × 88	280	50
(5)	MACS 0744	OVRO	49 × 55	100	56
(6)	MACS 1149	BIMA	101 × 87	290	50
(7)	MACS 1423	BIMA	103 × 87	240	40
(8)	MACS 2129	OVRO	53 × 57	80	40

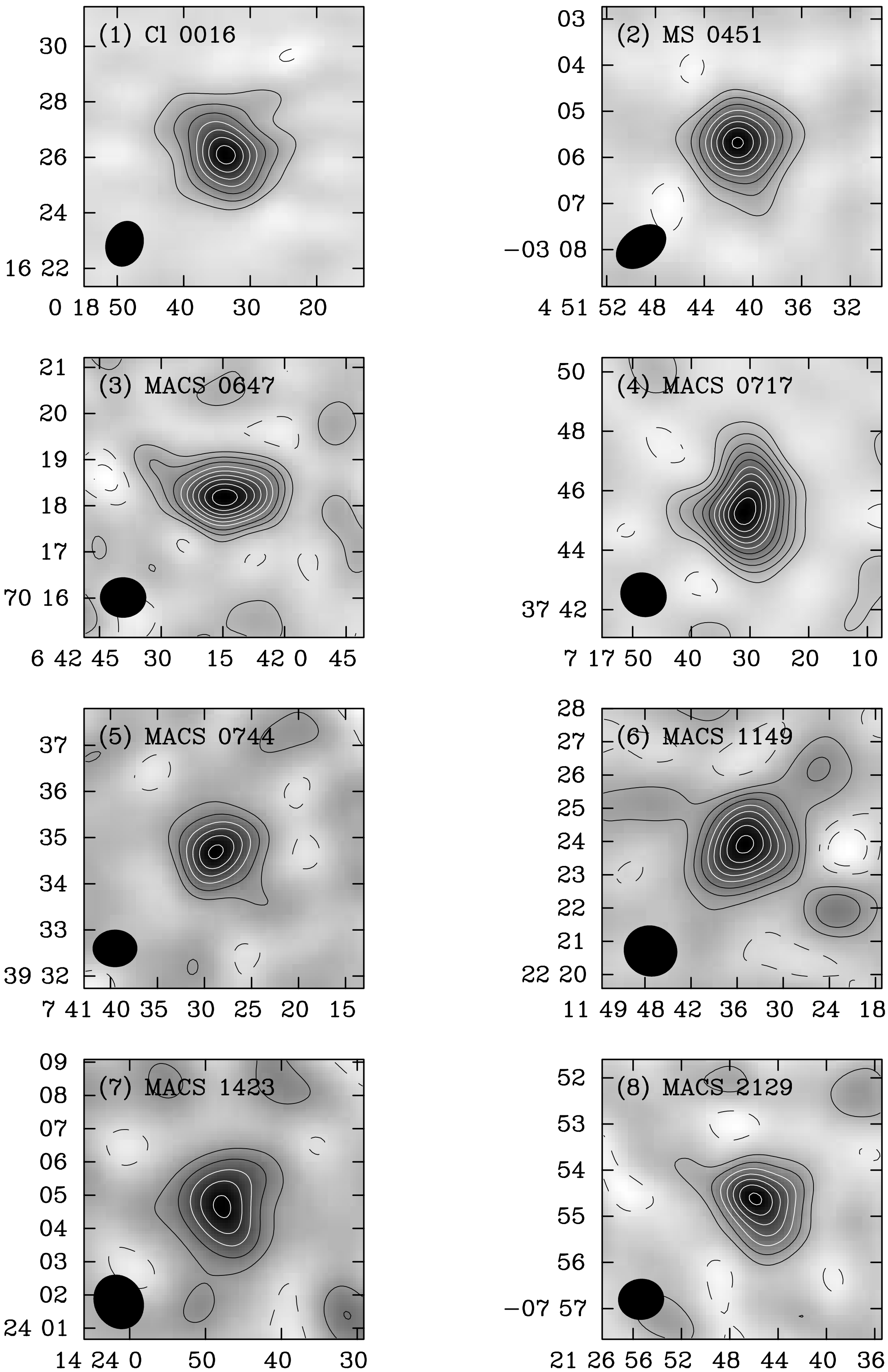

FIG. 1.—Synthesized images of the SZE decrement in the MACS clusters. All contours are multiples of 1.5 σ; BIMA images have a Gaussian taper of 1 kλ half-power radius applied to the *u-v* data. OVRO images have a taper of 2 kλ half-power radius applied. Additional image properties are summarized in Table 4. [*See the electronic edition of the Journal for a color version of this figure.*]

REFERENCES

Anders, E., & Grevesse, N. 1989, Geochim. Cosmochim. Acta, 53, 197
Bahcall, N. A., & Fan, X. 1998, ApJ, 504, 1
Carlstrom, J. E., Joy, M., & Grego, L. 1996, ApJ, 456, L75
Cavaliere, A., & Fusco-Femiano, R. 1976, A&A, 49, 137
———. 1981, A&A, 100, 194
Donahue, M. 1996, ApJ, 468, 79
Ebeling, H., Edge, A. C., & Henry, J. P. 2001, ApJ, 553, 668
Evrard, A. E. 1997, MNRAS, 292, 289
Evrard, A. E., Metzler, C. A., & Navarro, J. F. 1996, ApJ, 469, 494
Grego, L., Carlstrom, J. E., Joy, M. K., Reese, E. D., Holder, G. P., Patel, S., Cooray, A. R., & Holzapfel, W. L. 2000, ApJ, 539, 39
Grego, L., Carlstrom, J. E., Reese, E. D., Holder, G. P., Holzapfel, W. L., Joy, M. K., Mohr, J. J., & Patel, S. 2001, ApJ, 552, 2
Henry, J. P., Gioia, I. M., Maccacaro, T., Morris, S. L., Stocke, J. T., & Wolter, A. 1992, ApJ, 386, 408
Joy, M., LaRoque, S., Grego, L., Carlstrom, J. E., Dawson, K., Ebeling, H., Holzapfel, W. L., Nagai, D., & Reese, E. D. 2001, ApJ, 551, L1
Kaastra, J. S. 1992, in An X-Ray Spectral Code for Optically Thin Plasmas (Internal SRON-Leiden Report, updated version 2.0)
Koo, D. C. 1981, ApJ, 251, L75
Markevitch, M., Gonzalez, A. H., David, L., Vikhlinin, A., Murray, S., Forman, W., Jones, C., & Tucker, W. 2002, ApJ, 567, L27
Mewe, R., Gronenschild, E. H. B. M., & van den Oord, G. H. J. 1985, A&AS, 62, 197
Mewe, R., Lemen, J. R., & van den Oord, G. H. J. 1986, A&AS, 65, 511
Moffet, A. T., & Birkinshaw, M. 1989, AJ, 98, 1148
Mohr, J. J., Evrard, A. E., Fabricant, D. G., & Geller, M. J. 1995, ApJ, 447, 8
Morrison, R., & McCammon, D. 1983, ApJ, 270, 119
Neumann, D. M., & Böhringer, H. 1997, MNRAS, 289, 123
Pearson, T. J., Shepherd, M. C., Taylor, G. B., & Myers, S. T. 1994, BAAS, 185, 0808
Press, W. H., Teukolsky, S. A., Vetterling, W. T., & Flannery, B. P. 1992, Numerical Recipes in FORTRAN: The Art of Scientific Computing (2d ed.; Cambridge: Cambridge Univ. Press)
Reese, E. D., et al. 2000, ApJ, 533, 38
Rudy, D. J. 1987, Ph.D. thesis, Caltech
Sault, R. J., Teuben, P. J., & Wright, M. C. H. 1995, in ASP Conf. Ser. 77, Astronomical Data Analysis Software and Systems IV, ed. R. A. Shaw, H. E. Payne, & J. J. E. Hayes (San Francisco: ASP), 4, 433
Scoville, N. Z., Carlstrom, J. E., Chandler, C. J., Phillips, J. A., Scott, S. L., Tilanus, R. P. J., & Wang, Z. 1993, PASP, 105, 1482
Sunyaev, R. A., & Zeldovich, I. B. 1980, ARA&A, 18, 537
———. 1972, Comments Astrophys. Space Phys., 4, 173
Worrall, D. M., & Birkinshaw, M. 2003, MNRAS, submitted